Glycoconj J (2011) 28:183–196
DOI 10.1007/s10719-011-9333-6

N-Glycosylation profiling of recombinant mouse extracellular superoxide dismutase produced in Chinese hamster ovary cells

Hiroaki Korekane · Atsuko Korekane · Yoshiki Yamaguchi · Masaki Kato · Yasuhide Miyamoto · Akio Matsumoto · Tomoko Hasegawa · Keiichiro Suzuki · Naoyuki Taniguchi · Tomomi Ookawara

Received: 1 April 2011 / Revised: 28 April 2011 / Accepted: 29 April 2011 / Published online: 15 May 2011
© Springer Science+Business Media, LLC 2011

Abstract Extracellular superoxide dismutase (EC-SOD), the major SOD isoenzyme in biological fluids, is known to be *N*-glycosylated and heterogeneous as was detected in most glycoproteins. However, only one *N*-glycan structure has been reported in recombinant human EC-SOD produced in Chinese hamster ovary (CHO) cells. Thus, a precise *N*-glycan profile of the recombinant EC-SOD is not available. In this study, we report profiling of the *N*-glycan in the recombinant mouse EC-SOD produced in CHO cells using high-resolution techniques, including the liberation of *N*-glycans by treatment with PNGase F, fluorescence labeling by pyridylamination, characterization by anion-

Hiroaki Korekane and Atsuko Korekane contributed equally to this work.

Electronic supplementary material The online version of this article (doi:10.1007/s10719-011-9333-6) contains supplementary material, which is available to authorized users.

H. Korekane · T. Hasegawa · N. Taniguchi
Department of Disease Glycomics (Seikagaku Corporation), The Institute of Scientific and Industrial Research, Osaka University,
8–1 Mihogaoka,
Ibaraki, Osaka 567-0047, Japan

A. Korekane · T. Ookawara
Laboratory of Biochemistry, School of Pharmacy,
Hyogo University of Health Sciences,
1-3-6 Minatojima, Chuo-ku,
Kobe, Hyogo 650-8530, Japan

H. Korekane · Y. Yamaguchi · M. Kato · N. Taniguchi
Systems Glycobiology Research Group, Chemical Biology Department, Advanced Science Institute, RIKEN,
2-1 Hirosawa,
Wako, Saitama 351-0198, Japan

Y. Miyamoto
Department of Immunology,
Osaka Medical Center for Cancer and Cardiovascular Diseases,
1-3-2 Nakamichi,
Higashinari-ku, Osaka 537-8511, Japan

A. Matsumoto
Department of Pharmacology,
Chiba University Graduate School of Medicine,
1-8-1 Inohana,
Chuo-ku, Chiba 260-8670, Japan

K. Suzuki
Department of Biochemistry, Hyogo College of Medicine,
1-1 Mukogawa-cho,
Nishinomiya, Hyogo 663-8501, Japan

N. Taniguchi (✉)
Department of Disease Glycomics (Seikagaku Corporation), The Institute of Scientific and Industrial Research, Osaka University,
8-1 Mihogaoka,
Ibaraki, Osaka 567-0047, Japan
e-mail: tani52@wd5.so-net.ne.jp

N. Taniguchi
Systems Glycobiology Research Group, Chemical Biology Department, Advanced Science Institute, RIKEN,
2-1 Hirosawa,
Wako, Saitama 351-0198, Japan

T. Ookawara (✉)
Laboratory of Biochemistry, School of Pharmacy,
Hyogo University of Health Sciences,
1-3-6 Minatojima, Chuo-ku,
Kobe, Hyogo 650-8530, Japan
e-mail: biochook@huhs.ac.jp

exchange, normal and reversed phase-HPLC separation, and mass spectrometry. We succeeded in identifying 26 different types of *N*-glycans in the recombinant enzyme. The EC-SOD *N*-glycans were basically core-fucosylated (98.3% of the total *N*-glycan content), and were high mannose sugar chain, and mono-, bi-, tri-, and tetra-antennary complex sugar chains exhibiting varying degrees of sialylation. Four of the identified *N*-glycans were uniquely modified with a sulfate group, a Lewis^x structure, or an α-Gal epitope. The findings will shed new light on the structure-function relationships of EC-SOD *N*-glycans.

Keywords Chinese hamster ovary cells · Extracellular superoxide dismutase · *N*-Glycans · Pyridylamination · SOD3

Abbreviations

CBB	Coomassie brilliant blue
CHO	Chinese hamster ovary
dHex	deoxyhexose
ESI	electrospray ionization
Fuc	fucose
FUT	fucosyltransferase
Gal	galactose
GlcNAc	*N*-acetylglucosamine
GnT	*N*-acetylglucosaminyltransferase
GU	glucose units
Hex	hexose
HexNAc	*N*-acetylhexosamine
HPLC	high performance liquid chromatography
IT	ion-trap
Le^x	Lewis^x
Man	mannose
MS	mass spectrometry
NeuAc	*N*-acetylneuraminic acid
NP	normal phase
PA	pyridylaminated
PNGase F	peptide *N*-glycanase F
RP	reversed phase

Introduction

Superoxide radicals are formed in the greatest amounts during the metabolism of molecular oxygen. Superoxide is dismutated to hydrogen peroxide and oxygen by superoxide dismutases (SODs, EC 1.15.1.1), of which three isoenzymes have been identified in mammals. Copper-zinc SOD (Cu,Zn-SOD; SOD1) occurs in the cytosol [1], the intermembrane space of mitochondria [2], and the nucleus [3]. Manganese SOD (Mn-SOD; SOD2) is localized in the mitochondrial matrix [2, 4]. Extracellular SOD (EC-SOD; SOD3) is secreted into the extracellular space such as into the plasma, lymph, cerebrospinal fluid, and seminal plasma [5, 6], where it catalyzes the same enzymatic reaction as Cu,Zn-SOD [5, 7].

EC-SOD has a tetrameric structure, and shows affinity for heparin and other sulfated glycosaminoglycans [5, 8], and it is known that the major fraction of the enzyme in the body exists anchored to heparan sulfate proteoglycans in the tissue interstitium and on cell surfaces [9]. EC-SOD is known to be the only glycosylated SOD isoenzyme in mammals [5, 10], whereas naturally glycosylated Cu,Zn-SOD is known to be present in fungi [11, 12] and yeast [13]. A specific biological function of the *N*-glycan on EC-SOD has not been clearly identified yet [14].

It is well known that the glycosylation of proteins is the most common post-translational modification and has a strong effect on many of their functions, including cellular localization, turnover, protein quality control, and biological activities [15, 16]. Because the biosynthetic pathway involved in the construction of glycans comprises sequential and competitive steps involving glycoenzymes (glycosyltransferases and glycosidases), the glycan structure, when finally assembled on a glycoprotein, generally exhibits heterogeneity, reflected by the formation of a mixture of glycosylated variants, so called glycoforms. This heterogeneity is predicted to contribute to the functional diversity of individual glycoproteins. Although EC-SOD has a single *N*-glycosylation site [5, 10], the complex core-fucosylated biantennary sugar chain has only been identified in the case of recombinant human EC-SOD produced in CHO cells [10]. Thus, it is unclear whether or not the recombinant EC-SOD contains glycoforms. In order to understand the EC-SOD function, especially structure-function relationships related to its *N*-glycan, it is important to obtain a precise *N*-glycosylation profile of the enzyme.

In this study, we report *N*-glycosylation profiling of recombinant mouse EC-SOD produced in CHO cells using a variety of high-resolution techniques. We were able to identify a total of 26 major *N*-glycans in the recombinant mouse EC-SOD. They include one of the most predominant structures, a disialylated complex core-fucosylated biantennary sugar chain, previously reported to be present in recombinant human EC-SOD [10], and 25 additional types of *N*-glycans previously not revealed to be present in the recombinant enzyme. We also report the homology modeling of mouse EC-SOD.

Materials and methods

Standard pyridylaminated (PA)-oligosaccharides

The structures of and abbreviations for the authentic PA-oligosaccharides used in this study are listed in Supple-

mentary Table S1. The authentic oligosaccharides were obtained as follows: PA-[2,2]bi, PA-[2,2]biF, PA-[2,(2,4)]triF, PA-[(2,6),(2,4)]tetraF, PA-M3, and PA-M5A from Takara Bio Inc. (Shiga, Japan); PA-M3F, PA-[2,0]monoF, PA-[0,2]monoF, PA-ag[2,2]biF, PA-[2,2]biF-aG1, and PA-[2,2]biF-aG2 from Seikagaku Biobusiness Corp. (Tokyo, Japan); PA-$(\alpha G)_2$[2,2]biF was prepared from a purified porcine Na^+/K^+-ATPase; PA-ag[2,(2,4)]triF was prepared by digestion of PA-[2,(2,4)]triF with *Streptococcus pneumonia* β(1,4)-galactosidase (Prozyme, San Leandro, CA); PA-ag[(2,6),2]triF was enzymatically synthesized from PA-ag[2,2]biF by reaction with UDP-GlcNAc catalyzed by *N*-acetylglucosaminyltransferase V (GnT-V) [17] overexpressed in COS-1 cells; and PA-[(2,6),2]triF was synthesized from PA-ag[(2,6),2]triF by reaction with UDP-Gal catalyzed by a bovine milk β1,4-galactosyltransferase (Calbiochem-Novabiochem International Inc., La Jolla, CA, USA). The structures of PA-$(\alpha G)_2$[2, 2]biF, PA-ag[2,(2,4)]triF, PA-ag[(2,6),2]triF, and PA-[(2,6),2]triF were verified by normal and reversed phase HPLC analyses, combined with successive exoglycosidase digestions and by MS analysis (data not shown).

Preparation of recombinant mouse EC-SOD produced in CHO cells

The expression and purification of the recombinant mouse EC-SOD were carried out as described previously [18].

Gel electrophoresis

The purified recombinant mouse EC-SOD was subjected to SDS-PAGE under reducing conditions on a 12% gel according to the method of Laemmli [19], and protein bands were visualized by CBB staining.

Preparation of PA-*N*-glycans from recombinant mouse EC-SOD

The purified recombinant mouse EC-SOD (100 μg) was lyophilized, dissolved in 200 μl of alkylation buffer consisting of 7 M guanidine hydrochloride, 10 mM EDTA, and 0.5 M Tris-HCl buffer, pH 8.5, reduced with 10 mM DTT, S-carbamoylmethylated with 20 mM iodoacetamide, and then dialyzed against water. The dialyzed sample was again lyophilized, dissolved in 50 μl of 10 mM sodium phosphate buffer, pH 7.2, deglycosylated with 5U of PNGase F at 37°C for 24 h, and then deproteinated with 150 μl of ice-chilled ethanol. The supernatant, containing the liberated *N*-glycans, was evaporated, lyophilized, and then pyridylaminated by reductive amination [20]. Excess reagents were removed by phenol-chloroform extraction [21] and cation-exchange chromatography [22], followed by further purification by normal phase HPLC [23].

Preparation of a desialylated PA-*N*-glycan fraction

A one-tenth aliquot of the total PA-*N*-glycan fraction of the purified recombinant mouse EC-SOD was dissolved in 50 μl of 100 mM ammonium acetate buffer, pH 5.0, and then digested with 2 U/ml of *Arthrobacter ureafaciens* sialidase (Nacalai Tesque, Kyoto, Japan) at 37°C for 24 h. The reaction was terminated by boiling for 3 min, followed by centrifugation at 20,000 g for 5 min. The resulting supernatant was used as the desialylated PA-*N*-glycan fraction for structural analysis.

HPLC for structural analysis

Weak anion exchange HPLC was performed at 30°C on a TSKgel DEAE-5PW column (0.75×7.5 cm. Tosoh, Tokyo, Japan) at a flow rate of 0.8 ml/min. The solvents used were (A) aqueous ammonia, pH 9.0, and (B) 1 M ammonium acetate buffer, pH 9.0. The column was equilibrated with 100% solvent A and, after sample injection, solvent A was held at 100% for 0.5 min, and then solvent B was linearly increased to 14% in 17.5 min and then to 100% in 12.5 min. Fluorescence was monitored using excitation and emission wavelengths of 310 and 380 nm, respectively.

Reversed phase HPLC was performed at 30°C on a Cosmosil $5C_{18}$-P column (0.46×15 cm. Nacalai Tesque) at a flow rate of 1 ml/min. The solvents used were (A) 20 mM ammonium acetate buffer, pH 4.0, and (B) the same buffer containing 0.5% 1-butanol. The column was equilibrated with 5% solvent B and, after sample injection, solvent B was linearly increased to 100% in 70 min and then held at 100% for 5 min. Fluorescence was monitored using excitation and emission wavelengths of 320 and 400 nm, respectively.

Normal phase HPLC was performed at 40°C on a TSKgel Amide-80 column (3 μm, 0.46×15 cm. Tosoh) at a flow rate of 1 ml/min. The solvents used were (A) 100 mM triethylamine acetate buffer, pH 7.3, containing 90% acetonitrile and (B) 100 mM triethylamine acetate buffer, pH 7.3, containing 20% acetonitrile. The column was equilibrated with 5% solvent B and, after sample injection, solvent B was linearly increased to 75% over 40 min. Fluorescence was monitored using excitation and emission wavelengths of 310 and 380 nm, respectively.

The structures of the PA-oligosaccharides were determined by two-dimensional (2D) mapping [24, 25]. The retention time of each PA-oligosaccharide is given in glucose units (GU) based on the elution times of PA-isomaltooligosaccharides.

Exoglycosidase digestions

PA-oligosaccharides were digested in a volume of 20 μl for 16 h at 37°C using the following enzymes: *Streptococcus pneumonia* β-galactosidase (Prozyme), specificity for β(1-4)Gal, 0.1 U/ml in 50 mM sodium acetate buffer, pH 5.6; jack bean β-galactosidase (Seikagaku Biobusiness Corp.), specificity for β(1,4/3/6)Gal, 2 U/ml in 50 mM sodium citrate buffer, pH 3.6; *Streptomyces* sp.142 α-fucosidase (Takara Bio Inc.), specificity for α(1-3/4)Fuc, 0.2 mU/ml in 50 mM potassium phosphate buffer, pH 6.0; jack bean β-*N*-acetylhexosaminidase (Seikagaku Biobusiness Corp.), specificity for β(1-2/3/4/6)HexNAc, 2 U/ml in 50 mM sodium citrate buffer, pH 5.0; bovine kidney α-fucosidase (Sigma-Aldrich, ST. Louis, MO), specificity for α(1-2/3/4/6)Fuc, 0.5 U/ml in 50 mM sodium phosphate, pH 5.5; jack bean α-mannosidase (Seikagaku Biobusiness Corp.), specificity for α(1-2/3/6)Man, 2 U/ml in 50 mM sodium citrate buffer, pH 5.0, containing 2 mM $ZnCl_2$; and green coffee bean α-galactosidase (SIGMA-Aldrich), specificity for α(1-3/4/6)Gal, 4 U/ml in 50 mM sodium phosphate buffer, pH 6.5, in the presence of 0.1% of D-galactonic acid γ-lactone as a β-galactosidase inhibitor.

Methanolysis of sulfated PA-*N*-glycans

A sulfated PA-*N*-glycan was lyophilized and then subjected to methanolysis with 50 μl of 50 mM HCl dissolved in anhydrous methanol at 37°C for 3 h [26]. After concentration to dryness three times with 50 μl of anhydrous methanol, the product was re-*N*-acetylated with acetic anhydride in a saturated sodium bicarbonate solution for 30 min on ice. The reaction mixture was adsorbed to Dowex 50 W-X2 (H^+-form. Muromachi Kagaku Kogyo, Tokyo, Japan), eluted with 2.5% aqueous ammonia, and then evaporated to dryness. The sample was dissolved in water and then used for structural analysis.

Separation of sialylated and sulfated PA-*N*-glycans

Acidic glycans were found not to be separated with high resolution under our standard reversed phase HPLC conditions described formerly. Because of their negative charges, acidic glycans are generally not retained well with a reversed phase HPLC column compared with neutral glycans, and provide broad ambiguous peaks and a bad separation on reversed phase HPLC. The use of one of the classic ion-pair reagents, triethylamine, was found to improve retention and separation of acidic glycans on reversed phase HPLC. Thus, we used another reversed phase HPLC condition for separation and collection of acidic glycans as follows. The separation of sialylated and sulfated PA-*N*-glycans was performed at 30°C on a Cosmosil $5C_{18}$-P column (0.46×15 cm. Nacalai Tesque) at a flow rate of 1 ml/min. The solvents used were (A) 20 mM triethylamine acetate buffer, pH 4.0, and (B) the same buffer containing 1% 1-butanol. The column was equilibrated with 2.5% solvent B and, after sample injection, solvent B was linearly increased to 80% in 70 min and then held at 80% for 5 min. Fluorescence was monitored using excitation and emission wavelengths of 320 and 400 nm, respectively.

Electorospray ionization MS analysis

Mass spectra of PA-oligosaccharides were obtained on a Finnigan LCQ Deca XP ion-trap mass spectrometer (ThermoFischer Scientific, Waltham, MA) equipped with a nanoESI device (AMR, Tokyo, Japan) connected to a Paradigm MS4 μHPLC system (Michrom BioResources Inc., CA) equipped with a Magic C18 column (0.2×5 cm. Michrom BioResources Inc.), as previously described [27].

Homology modeling of mouse EC-SOD

Homology modeling was performed using the Modeller 9v7 software program [28]. The crystal structure of human EC-SOD [29] (PDB code 2JLP) was used as a template for the modeling. The disulfide-bonding pattern of mouse EC-SOD was obtained from the UniProt database [30]. *N*-Glycans on Asn-97 [31] were modeled with GlyProt (http://www.glycosciences.de/glyprot/) and a figure was prepared using Pymol software (http://www.pymol.org/).

Results

Preparation of PA-*N*-glycans from recombinant mouse EC-SOD

In order to determine the precise *N*-glycan profile in the recombinant mouse EC-SOD, we purified it from conditioned medium of CHO-EK cells, which were stably producing and secreting the recombinant protein [18]. SDS-PAGE analysis of the purified enzyme fraction gave two bands corresponding to molecular weights of 33 K and 35 K (Supplementary Fig. S1). Both materials were confirmed to be mouse EC-SOD subunits [32]. *N*-Glycans in the recombinant mouse EC-SOD were released by cleavage with PNGase F and the reducing ends of the liberated *N*-glycans were pyridylaminated. The resulting PA-*N*-glycans were used for the structural analyses described below.

The core structure of PA-*N*-glycans in recombinant mouse EC-SOD

To unequivocally determine the *N*-glycan structures, an aliquot of the total PA-*N*-glycans obtained was desialylated

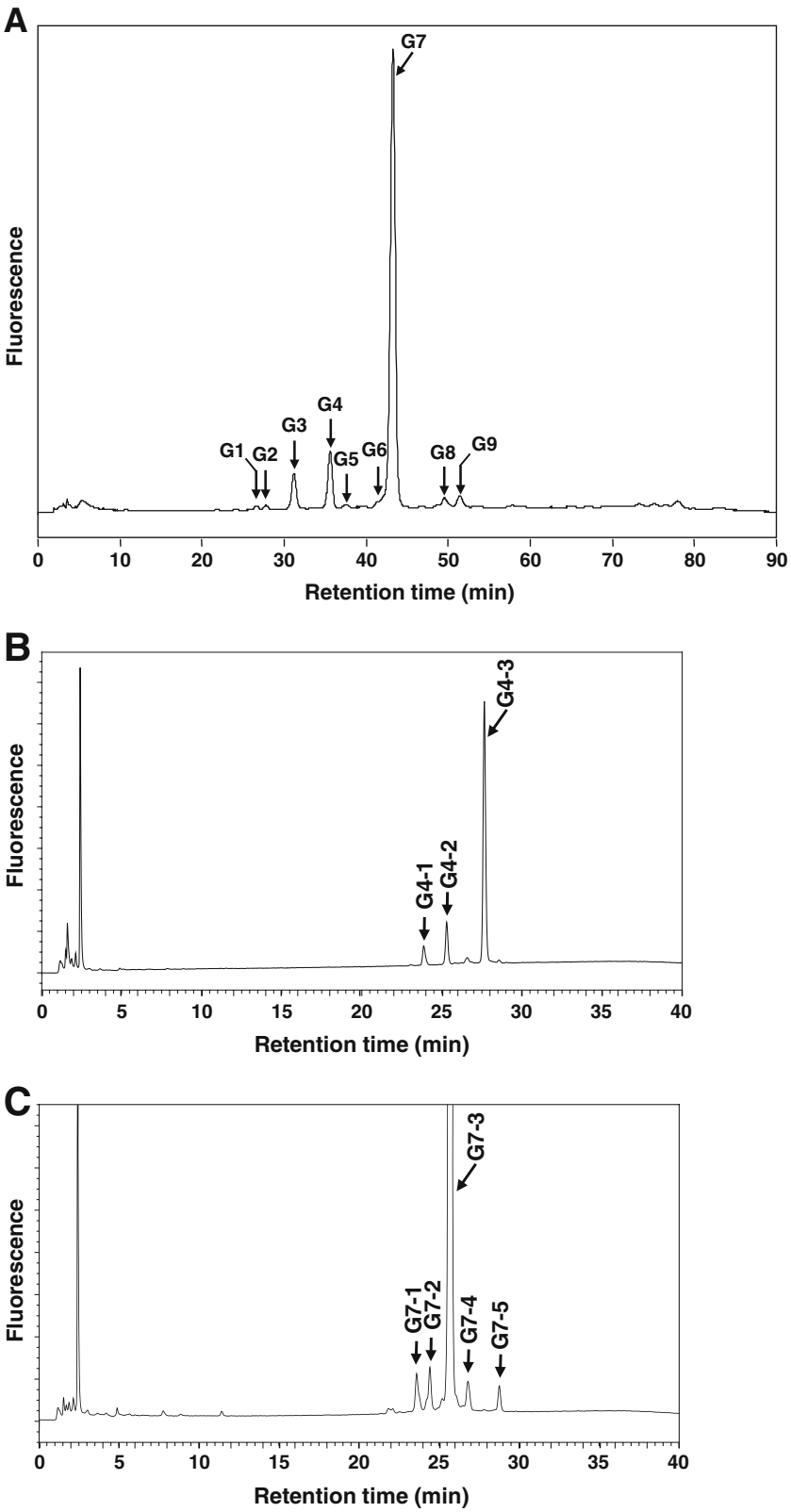

Fig. 1 Separation of desialylated PA-*N*-glycans derived from recombinant mouse EC-SOD. **a**. Reversed phase HPLC elution profile of the desialylated PA-*N*-glycans. A total of nine peaks, denoted as G1 to G9 and indicated by *arrows*, were detected. **b**. G4 in panel A was further separated by normal phase HPLC. A total of three peaks, denoted as G4-1 to G4-3 and indicated by *arrows*, were detected. **c**. Elution profile of G7 in panel A on normal phase HPLC. A total of five peaks, denoted as G7-1 to G7-5 and indicated by *arrows*, were detected. Peaks at 1–3 min in panels B and C were due to contaminating materials

by treatment with *Arthrobacter ureafaciens* sialidase, and then the digested products were separated by reversed phase (RP) HPLC (Fig. 1a), the PA-oligosaccharides being separated according to their oligosaccharide structure. A

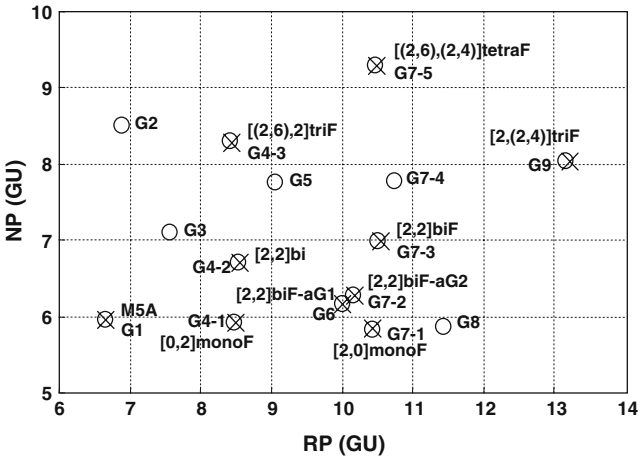

Fig. 2 Two-dimensional map of the core structures of the PA-*N*-glycans derived from the recombinant mouse EC-SOD. The elution profile of each PA-*N*-glycan on normal and reversed phase HPLC is expressed in glucose units (GU) based on the elution times of PA-isomaltooligosaccharides and plotted on the map. The *circles* indicate the positions of the peaks. *Xs* indicate the positions of the standard PA-oligosaccharides (Table S1). NP, normal phase; RP, reversed phase

total of nine major peaks (G1-G9) was obtained, each of which was further separated by normal phase (NP) HPLC, the PA-oligosaccharides being separated based on molecular size. As shown in Fig. 1b and c, G4 and G7 were further separated into three and five major peaks, respectively, designated as G4-1, G4-2, G4-3, G7-1, G7-2, G7-3, G7-4, and G7-5, by NP-HPLC. The elution positions of these PA-*N*-glycans on RP- and NP-HPLC are summarized in Fig. 2 in the form of a two-dimensional (2D) map. From the positions on the map corresponding to authentic PA-oligosaccharides (Table S1), G1, G4-1, G4-2, G4-3, G6, G7-1, G7-2, G7-3, G7-5, and G9 were determined to be PA-M5A, PA-[0,2]monoF, PA-[2, 2]bi, PA-[(2,6),2]triF, PA-[2, 2]biF-aG1, PA-[2,0]monoF, PA-[2, 2]biF-aG2, PA-[2,2]biF, PA-[(2,6),(2,4)]tetF, and PA-[2,(2,4)]triF, respectively. These structures were also confirmed by MS analysis (Table 1). The structures of G2, G3, G5, G7-4, and G8 were determined by the 2D-mapping technique combined with appropriate linkage-specific exoglycosidase digestions, chemical treatment, and MS analysis as follows.

Structures of G2 and G3

G2 and G3 were determined to be C2 epimerization products of G4-3 and G7-3, respectively. The results are shown in Supplementary Fig. S2 and Doc. S1.

Structure of G5

G5, which had the composition $Hex_5HexNAc_4dHex_2$-PA (Table 1), was sequentially digested with linkage-specific exoglycosidases in the following reaction order: 1st *Streptococcus pneumonia* β(1,4)-galactosidase, *Streptomyces* sp142 α(1,3/4)-fucosidase, and 2nd *Streptococcus pneumonia* β(1,4)-galactosidase (Fig. 3a). A single residue was removed at each step, indicating the presence of one Lewis^x (Le^x) structure with a fucose linked via an α(1-3) linkage to GlcNAc (the presence of a Fuc residue renders the Gal residue resistant to cleavage). The elution positions

Table 1 Mass analysis of PA-*N*-glycans derived from the recombinant mouse EC-SOD

Peak	Mass		Determined composition
	Observed	Calculated	
G1	1313.5 (H^+)	1313.5 (H^+)	$Hex_5HexNAc_2$-PA
G7-1	1500.5 (H^+)	1500.6 (H^+)	$Hex_4HexNAc_3dHex_1$-PA
G4-1	1500.7 (H^+)	1500.6 (H^+)	$Hex_4HexNAc_3dHex_1$-PA
G6	1703.7 (H^+)	1703.7 (H^+)	$Hex_4HexNAc_4dHex_1$-PA
G7-2	1703.6 (H^+)	1703.7 (H^+)	$Hex_4HexNAc_4dHex_1$-PA
G4-2	1719.6 (H^+)	1719.7 (H^+)	$Hex_5HexNAc_4$-PA
G7-3	1865.6 (H^+)	1865.7 (H^+)	$Hex_5HexNAc_4dHex_1$-PA
G3	1865.8 (H^+)	1865.7 (H^+)	$Hex_5HexNAc_4dHex_1$-PA
G8	1967.5 (Na^+)	1967.7 (Na^+)	$(HSO_3)_1Hex_5HexNAc_4dHex_1$-PA
G5	2011.7 (H^+)	2011.8 (H^+)	$Hex_5HexNAc_4dHex_2$-PA
G7-4	2027.7 (H^+)	2027.8 (H^+)	$Hex_6HexNAc_4dHex_1$-PA
G9	2230.7 (H^+)	2230.8 (H^+)	$Hex_6HexNAc_5dHex_1$-PA
G2	2230.6 (H^+)	2230.8 (H^+)	$Hex_6HexNAc_5dHex_1$-PA
G4-3	2230.7 (H^+)	2230.8 (H^+)	$Hex_6HexNAc_5dHex_1$-PA
G7-5	2595.7 (H^+)	2595.9 (H^+)	$Hex_7HexNAc_6dHex_1$-PA
S4a	2549.5 (Na^+)	2549.8 (Na^+)	$NeuAc_2(HSO_3)_1Hex_5HexNAc_4dHex_1$-PA
S4b	3758.0 (H^+)	3760.4 (H^+)	$NeuAc_4Hex_7HexNAc_6dHex_1$-PA

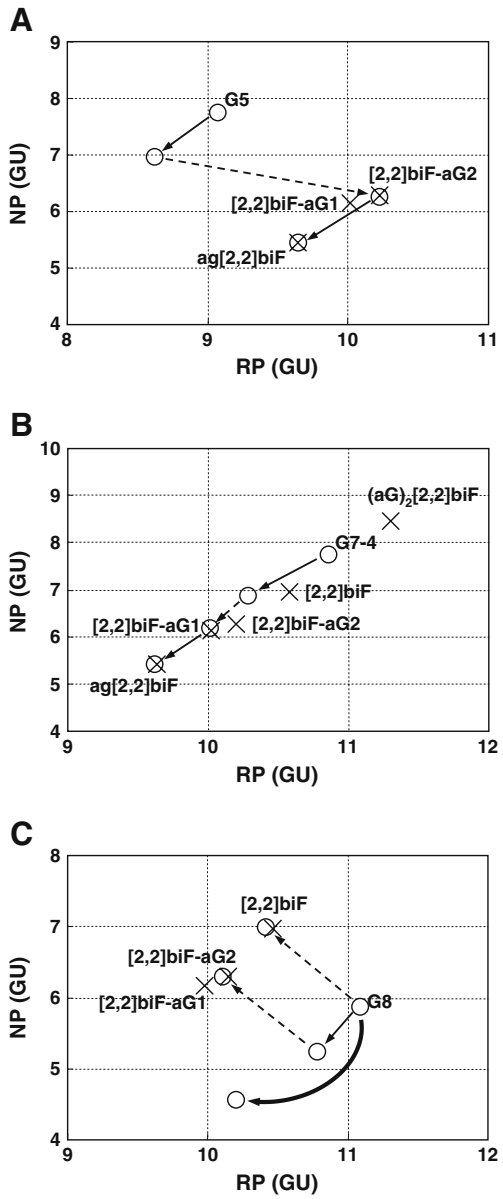

◀ **Fig. 3** Analyses of G5, G7-4, and G8 by exoglycosidase digestions or methanolysis. **a**. Map of G5. Circles indicate the elution positions of G5 and its digests. *Solid arrows* indicate the direction of change in the elution positions on digestion with a β1,4-galactosidase. The *dotted arrow* indicates the direction of change in the elution position on digestion with an α1,3/4-fucosidase. **b**. Map of G7-4. *Solid arrows* indicate the direction of change in the elution positions on digestion with a β1,4-galactosidase. The *dotted arrow* indicates the direction of change in the elution position on digestion with an α1,3/4/6-galactosidase. **c**. Map of G8. *Circles indicate* the elution positions of G8, its digests, and methanolysates. *Thin* and *thick arrows* indicate the directions of the changes in the elution positions on digestion with the *Streptococcus pneumonia* and jack bean β-galactosidases, respectively. The *dotted arrows* indicate the directions of the changes in the elution positions after methanolysis. *Xs* indicate the positions of the standard PA-oligosaccharides (Table S1). NP, normal phase; RP, reversed phase. The contributions of monosaccharide units to GU values on normal phase HPLC are as follows. β-Galactose ca. 0.7-0.9 GU; Lewis-type α-fucose ca. 0.7 GU; and α-galactose ca. 0.7 GU. The assignment was made according to the decrease in the NP-GU value observed on the removal of a monosaccharide unit by exoglycosidase digestion from the standard PA-oligosaccharide (data not shown)

on the map of the digested products were shifted to positions corresponding to authentic PA-oligosaccharides PA-[2,2]biF-aG2 and ag[2,2]biF after digestion with the α-fucosidase and the 2nd β-galactosidase, respectively. Thus, the structure of G5 was determined to be PA-[2,2]biF with one Le^x structure on the Manα(1-3) arm of the complex core-fucosylated biantennary sugar chain.

Structure of G7-4

G7-4, which had the composition $Hex_6HexNAc_4dHex_1$-PA (Table 1), was sequentially digested with the 1st *Streptococcus pneumonia* β(1,4)-galactosidase, green coffee bean α(1,3/4/6)-galactosidase, and 2nd *Streptococcus pneumonia* β(1,4)-galactosidase (Fig. 3b). A single residue was removed at each step, indicating the presence of one α-Gal residue linked to a Galβ(1-4) residue. The elution positions on the map of the digested products were shifted to positions corresponding to authentic PA-oligosaccharides PA-[2,2]biF-aG1 and ag[2,2]biF after digestion with the α-galactosidase and the 2nd β-galactosidase, respectively. Thus, the structure of G7-4 was determined to be PA-[2,2]biF with one α-Gal epitope on the Manα(1-6) arm of the complex core-fucosylated biantennary sugar chain.

Structure of G8

G8 exhibited an *m/z* at 1967.5, corresponding to $[(HSO_3)_1$-$Hex_5HexNAc_4dHex_1$-PA + $Na]^+$ (Table 1), suggesting that G8 was a sulfated *N*-glycan. To determine the core structure of G8, the molecule was subjected to methanolysis. The methanolyzed product was eluted at the same position as authentic PA-oligosaccharide PA-[2,2]biF as shown on NP- and RP-HPLC analyses (Fig. 3c, and Supplementary Fig. S3A and B). It has been reported that jack bean β(1,4/3/6)-galactosidase catalyzes the hydrolysis of the Galβ1-4 (HSO_3-6)GlcNAc structure, whereas such a structure is resistant to the action of *Streptococcus pneumonia* β(1,4)-galactosidase [26, 33]. As shown in Fig. 3c, when G8 was digested with *Streptococcus pneumonia* β-galactosidase, the molecular size of the digested product was decreased by 0.64 NP-GU, indicating that one galactose residue bound to the unsulfated GlcNAc residue was hydrolyzed. On the other hand, a decrease in GU was observed, corresponding to the removal of two galactose residues (1.33 NP-GU), on the digestion of G8 with jack bean β-galactosidase, indicating again that this glycan contained a sulfated GlcNAc residue. To confirm the position of the sulfate

group, linkage-specific exoglycosidase digestion and methanolysis were combined with 2D-mapping (Fig. 3c). G8 was digested with *Streptococcus pneumonia* β-galactosidase and then subjected to methanolysis. The elution position of the product on the map was shifted to a position corresponding to authentic PA-oligosaccharide PA-[2,2]biF-aG2, indicating that the sulfate residue was linked to a GlcNAc residue on the Manα(1-3) arm of the complex core-fucosylated biantennary sugar chain. The determined core structures of the PA-*N*-glycans derived from the recombinant mouse EC-SOD are shown in Supplementary Table S2. The determined core structures of PA-*N*-glycans were used as standard PA-oligosaccharides in the following analyses.

Acidic character of PA-N-glycans derived from recombinant mouse EC-SOD

To confirm the pattern of NeuAc substitution of the PA-*N*-glycans, the total PA-*N*-glycans were separated by DEAE-HPLC without desialylation (Fig. 4a). The PA-*N*-glycans were separated into neutral (N), mono- (S1), di- (S2), tri- (S3), and tetra-sialyl (S4) fractions. After desialylation with *Arthrobacter ureafaciens* sialidase, each fraction was separated by RP-HPLC, as shown in Fig. 4b. A total of 20 major PA-*N*-glycan peaks were separated and collected, followed by further separation by NP-HPLC. Peaks N2, N3', N4, S1-2, S1-3, S1-4, and S2-3 were further separated into two to four peaks, designated as N2a, N2b, N2c, N3'a, N3'b, N4a, N4b, N4c, N4d, S1-2a, S1-2b, S1-2c, S1-3a, S1-3b, S1-4a, S1-4b, S1-4c, S1-4d, S2-3a, and S2-3b, by NP-HPLC (data not shown). The elution positions of these separated PA-*N*-glycans on RP- and NP-HPLC were 2D-mapped, and compared with those obtained for the predetermined core structures (Table S2 and Fig. 5), and then their acidic characteristics were examined. Because a sulfate residue itself has an acidic nature, sulfated PA-*N*-glycan S4-2 was further analyzed by MS to determine its precise acidic characteristics. The total S4 fraction (Fig. 4a) was separated into two major peaks, S4a and S4b, by RP-HPLC (Supplementary Fig. S4) and then analyzed by MS. As shown in Table 1, the compositions of S4a and S4b were determined to be $NeuAc_2(HSO_3)_1Hex_5HexNAc_4dHex_1$-PA and $NeuAc_4Hex_7HexNAc_6dHex_1$-PA, respectively. Accordingly, S4a was found to be a disialylated and monosulfated complex core-fucosylated biantennary sugar chain. The 26 different types of *N*-glycans identified in this study are summarized in Table 2.

Discussion

In the present study, we were able to identify 26 major types of *N*-glycans that are expressed in recombinant mouse EC-SOD. The disialylated complex core-fucosylated biantennary sugar chain was found to be the predominant *N*-glycan (55.7% of the total *N*-glycan content, Table 2, S2 [2,2]biF) in the recombinant mouse EC-SOD, a finding that is consistent with previously reported results for recombinant human EC-SOD [10]. Furthermore, 25 additional types of *N*-glycans were found to be present in the recombinant mouse EC-SOD. The *N*-glycans in the recombinant mouse EC-SOD were found to be basically core-fucosylated (98.3% of the total *N*-glycan content, Table 2), indicating that the EC-SOD is one of the most efficient target proteins [34] for the reaction catalyzed by

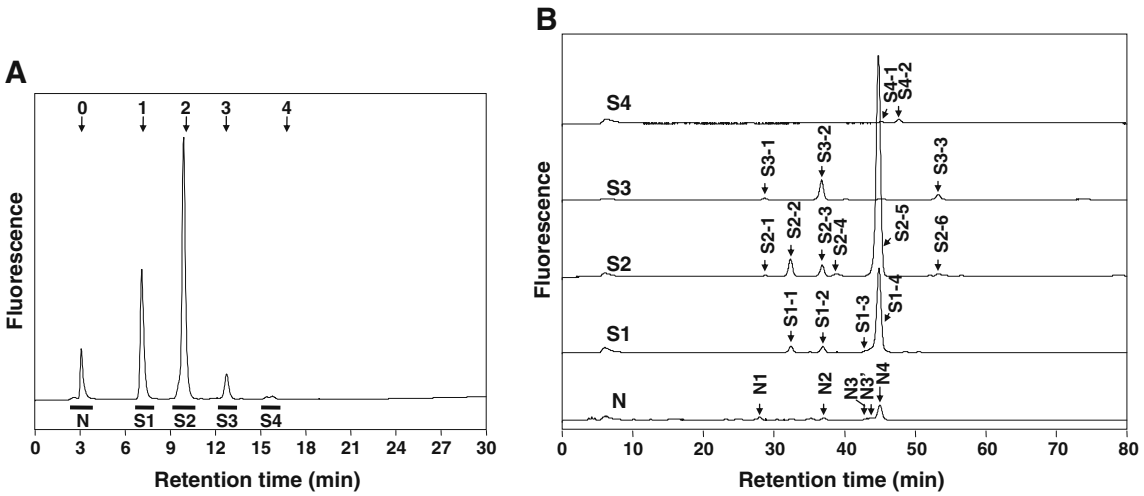

Fig. 4 Weak anion-exchange and reversed phase HPLC of PA-*N*-glycans derived from the recombinant mouse EC-SOD. **a**. PA-*N*-glycans were separated into five fractions (N, S1, S2, S3, and S4) by DEAE-HPLC. The numbered arrows indicate the elution positions of the standard PA-*N*-glycans with the corresponding numbers of sialic acid residues. **b**. After desialylation by treatment with *Arthrobacter ureafaciens* sialidase, each fraction was further separated by reversed phase HPLC. The separated peaks are indicated by arrows

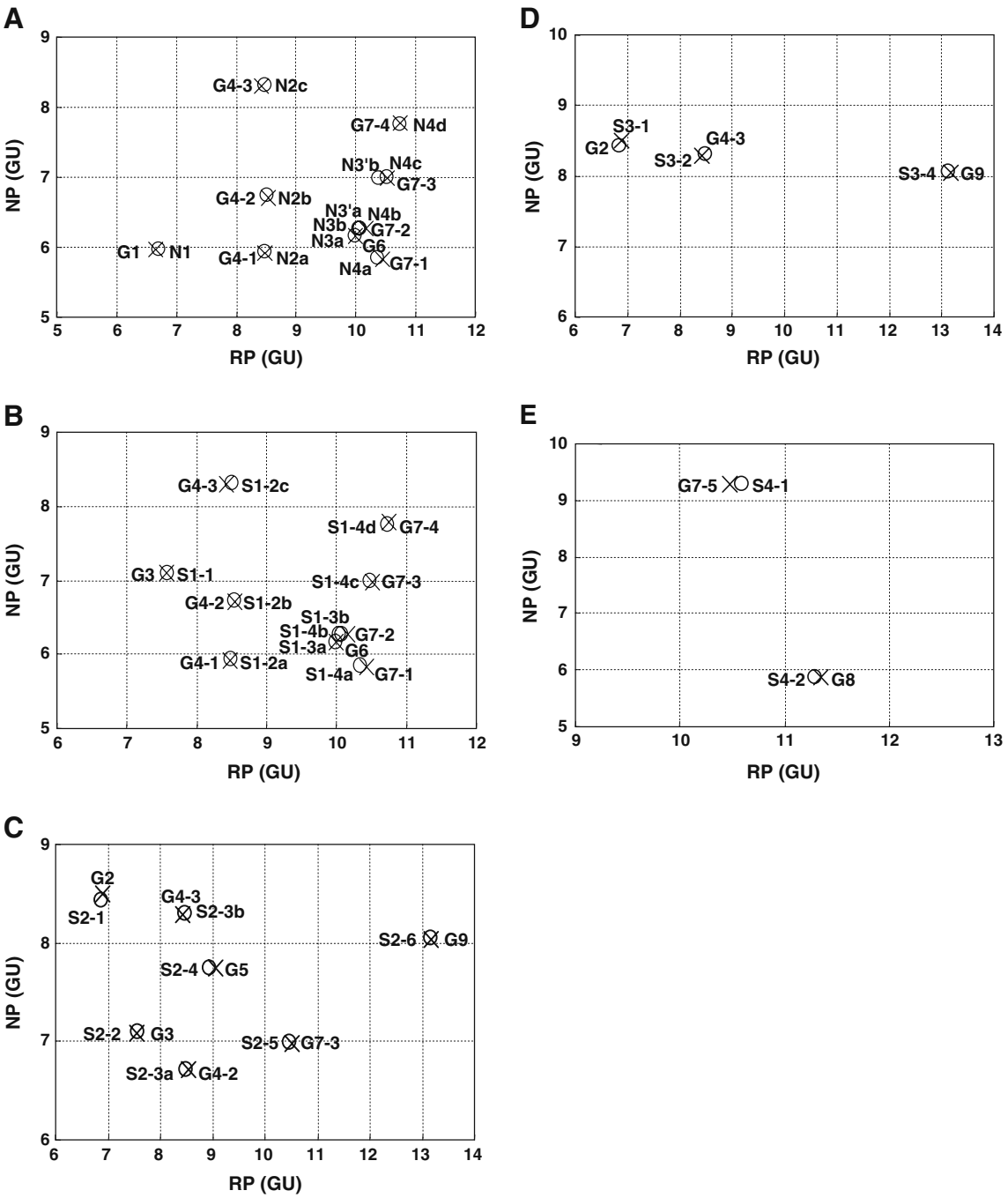

Fig. 5 Two-dimensional maps of PA-*N*-glycans derived from the recombinant mouse EC-SOD. Maps of the core structures of PA-*N*-glycans separated into the N fraction (**a**), S1 fraction (**b**), S2 fraction (**c**), S3 fraction (**d**), and S4 fraction (**e**), respectively, in Fig. 4a. The *circles* indicate the positions of the peaks. *Xs* indicate the positions of the pre-determined core structures of PA-*N*-glycans in the recombinant mouse EC-SOD (Table S2)

α1,6-fucosyltransferase (FUT8) [35], the only known enzyme that is able to catalyze the core-fucosylation reaction. Regarding GlcNAc branch formation, mono-, bi-, tri-, and tetra-antennary complex sugar chains were found to be present in percent ratios of 1.1, 87.2, 10.7, and 0.4, respectively. Thus, a typical biantennary sugar chain was the most predominant, bulky tri- and tetra-antennary sugar chains being the second most abundant *N*-glycans in the recombinant mouse EC-SOD (Table 2). The presence of tri- and tetra-antennary sugar chains indicates that the EC-SOD is also the target protein for the reactions catalyzed by GnT-IV [36] and GnT-V [17], and that these bulky high-branched *N*-glycans might have functions that are different from that of the typical biantennary sugar chain. For

Table 2 Determined structures of PA-*N*-glycans derived from the recombinant mouse EC-SOD

Peak	Structure	Abbreviation	Ratio (%)
	(Neutral)		
G1	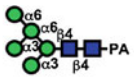	**M5A**	**0.6**
G4-1	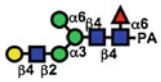	**[0,2]moF**	**0.1**
G4-2	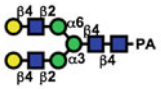	**[2,2]bi**	**0.2**
G4-3	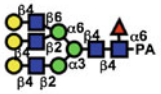	**[(2,6),2]triF**	**0.2**
G6	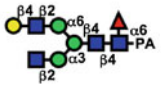	**[2,2]biF-aG1**	**0.3**
G7-1	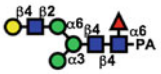	**[2,0]moF**	**0.3**
G7-2	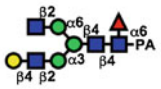	**[2,2]biF-aG2**	**0.5**
G7-3	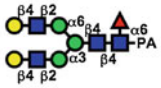	**[2,2]biF**	**4.3**
G7-4	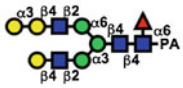	**(αG)$_1$[2,2]biF**	**0.1**
	(Monosialo)		
S1G4-1	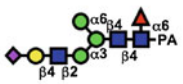	**S1[0,2]moF**	**0.3**
S1G4-2	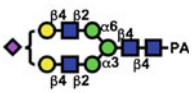	**S1[2,2]bi**	**0.5**
S1G4-3	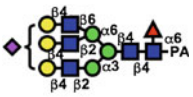	**S1[(2,6),2]triF**	**0.7**
S1G6	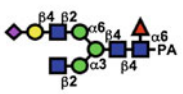	**S1[2,2]biF-aG1**	**0.4**
S1G7-1	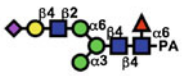	**S1[2,0]moF**	**0.4**
S1G7-2	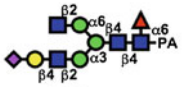	**S1[2,2]biF-aG2**	**0.8**
S1G7-3	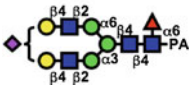	**S1[2,2]biF**	**21.6**

S1G7-4	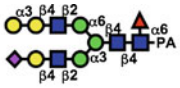	**S1(αG)$_1$[2,2]biF**	**0.6**
	(Disialo)		
S2G4-2	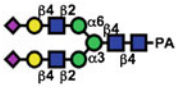	**S2[2,2]bi**	**0.4**
S2G4-3	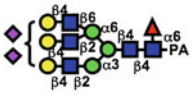	**S2[(2,6),2]triF**	**2.2**
S2G5	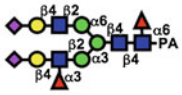	**S2(Le^x)$_1$[2,2]biF**	**0.7**
S2G7-3	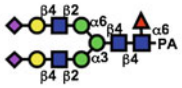	**S2[2,2]biF**	**55.7**
S2G9	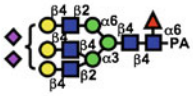	**S2[2,(2,4)]triF**	**0.7**
	(Trisialo)		
S3G4-3	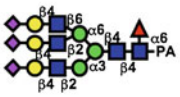	**S3[(2,6),2]triF**	**5.2**
S3G9	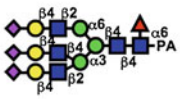	**S3[2,(2,4)]triF**	**1.7**
	(Tetrasialo)		
S4G7-5	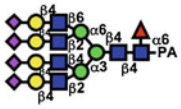	**S4[(2,6),(2,4)]tetF**	**0.4**
	(Sulfo)		
(HSO$_3$)$_1$G8	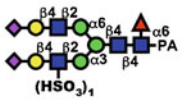	**S2(HSO$_3$)$_1$[2,2]biF**	**1.1**

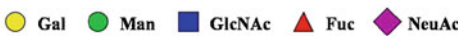

example, our previous study revealed that the formation of a β(1-6)GlcNAc branch, which is catalyzed by the action of GnT-V, in the *N*-glycan at Asn-772 in matriptase makes the protein more resistant to tryptic digestion, compared to the control matriptase with no β(1-6)GlcNAc branching [37], indicating that β(1-6)GlcNAc-branch formation contributes to the stability of the protein. Similar proteolytic stability of the EC-SOD modified with a β(1-6)GlcNAc-branched *N*-glycan is a distinct possibility and, if so, the enzyme may have a longer half-time in the plasma than the enzyme with the typical biantennary sugar chain. We further examined the acidic character of EC-SOD *N*-glycans, 93.4% of the *N*-glycans being found to be modified through mono-, di-, tri-, or tetra-sialylation (Table 2), though the type of sialyl-

linkages such as sialylα2-6Gal or sialylα2-3Gal could not be determined in this study because of the limitation of the sample amount. In addition, in a small fraction of the total *N*-glycan content (2.5%, Table 2), four types of *N*-glycans were found to be uniquely modified with a sulfate group, a Le^x structure, or an α-Gal epitope (Table 2, $S2(HSO_3)_1$[2,2]biF, $S2(Le^x)_1$[2,2]biF, $S1(\alpha G)_1$[2,2]biF, and $(\alpha G)_1$[2,2]biF).

Concerning the significance of *N*-glycosylation in EC-SOD, Edlund *et al*. previously constructed a non-glycosylated form of recombinant human EC-SOD by site-directed mutagenesis at its potential *N*-glycosylation site of Asn-89, which was substituted with a Gln residue, and compared the properties of the product, including enzyme activity, heparin binding, solubility, and plasma clearance *in vivo*, with those of the wild-type recombinant human EC-SOD [14]. Although they concluded that no specific biological role for the EC-SOD *N*-glycan could be clearly elucidated, small but distinct differences in heparin binding affinity and the plasma clearance rate *in vivo* between the mutant and the wild-type EC-SODs were detected. The mutant enzyme showed a slightly higher binding affinity to heparin and a slightly more rapid turnover rate *in vivo* compared to the wild-type enzyme, suggesting that the *N*-glycosylation in EC-SOD could alter its function in at least these two EC-SOD properties. In the primary sequence of EC-SOD, the *N*-glycosylation site is located near the central part, distant from its heparin-binding domain, which is at the C-terminal end [38]. Antonyuk *et al.* quite recently succeeded in determining the first crystal structure of the recombinant human EC-SOD at a resolution of 1.7Å, and presented simulated docking models of heparin and collagen binding to EC-SOD [29]. They proposed, in their calculated docking models, that the two grooves formed by the tetramer interface of the EC-SOD were probable binding sites for heparin and collagen, and the Asn-89*N*-glycosylation sites were located on the surface of the tetramer at the ends of each groove, offering a probable explanation for why the heparin binding affinity was different between the non-glycosylated and glycosylated recombinant EC-SODs in the previous study [14]. Our own structural modeling of the mouse EC-SOD tetramer showed that the Asn-97*N*-glycosylation sites [31] are located on the surface of the protein with the attached *N*-glycans exposed to the solvent (Fig. 6), a situation that would reasonably contribute to increasing the solubility of the enzyme in an aqueous environment, and that is consistent with the reported reduction in the solubility of the non-glycosylated human recombinant EC-SOD [14]. It is assumed that the EC-SOD protein face to which the *N*-glycan is attached would always be exposed to the outer solvent, and would not to be used in the formation of the inside subunit-subunit interface of the EC-SOD tetramer. This suggests that the EC-SOD *N*-glycans may play a role in the efficient assembly of the enzyme subunits into the tetramer by arranging each subunit in the correct orientation in an aqueous environment. Due *et al.* interestingly reported that EC-SOD purified from the human aorta is present as two distinct quaternary structures, a major population of a tetrameric EC-SOD and a minor population of an octameric enzyme, the latter of which is estimated to comprise about 1% of the total enzyme content [39]. They found that the EC-SOD octamer shows an increased affinity for heparin binding and an increased conformational stability, as assessed by denaturant-induced unfolding, as compared to those of the tetrameric enzyme, indicating that the formation of an octameric structure of EC-SOD induces changes in the properties of the enzyme. The involvement of EC-SOD *N*-glycans in the formation of the EC-SOD octamer has not been examined. It would be worth examining whether the EC-SOD *N*-glycans are responsible for the octamer formation and/or the resulting changes in the enzyme properties.

It is well known that EC-SOD is expressed at high levels in the lungs and vessels [40–42]. Studies on mice lacking EC-SOD indicated that the enzyme plays multiple roles in various pathophysiologic conditions, including the protection of the lungs against hyperoxia [43], reduction of angiotensin-2-induced hypertension [44], and acceleration of neovascularization [45]. In addition, Yao *et al*. quite recently reported that EC-SOD plays a role in protecting the lungs against emphysema induced in mice by cigarette smoking or elastase treatment, which is attributed to a

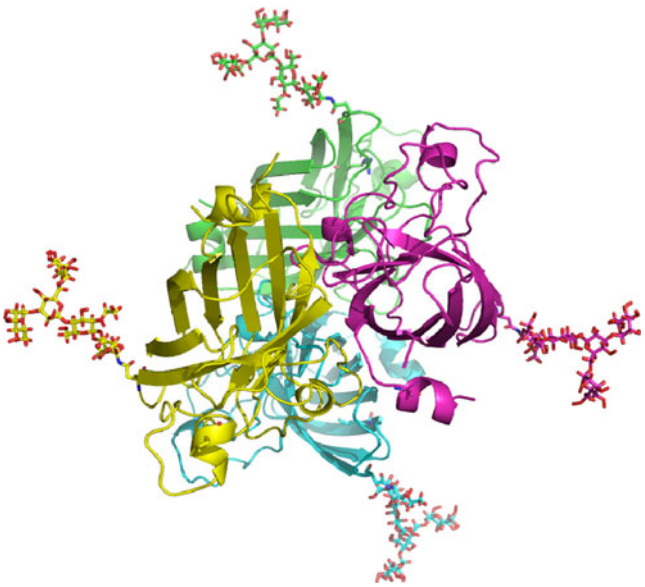

Fig. 6 Structural model of mouse EC-SOD. A structural model of the mouse EC-SOD tetramer was constructed based on the crystal structure of human EC-SOD [29] (see Materials and Methods). The structure is shown as a ribbon model, and the subunits are colored green, cyan, magenta and yellow, respectively. *N*-Glycans attached to Asn-97 are shown as a stick model

reduction in the extent of oxidative fragmentation of the extracellular matrix (ECM) in the lungs [46]. We previously reported that *Fut8* knockout (*Fut8*$^{-/-}$) mice exhibit emphysema-like changes in the lungs that appear to be partly due to a lack of core-fucose in the TGF-β1 receptor, which consequently results in marked dysregulation of TGF-β1 receptor activation and signaling, causing a failure to control ECM homeostasis by down-regulating matrix metalloproteinases (MMPs) [47]. In the present study, EC-SOD was found to be an efficient target protein for the core-fucosylation reaction catalyzed by FUT8. The EC-SOD in *Fut8*$^{-/-}$ mouse lungs is predicted to be naturally present as a non-core-fucosylated form. It would be of interest to compare the enzyme properties of the core-fucosylated and non-core-fucosylated EC-SODs, and to determine whether or not the non-core-fucosylated EC-SOD contributes to any extent to the development of the emphysema-like changes in *Fut8*$^{-/-}$ mice.

In summary, a variety of high-resolution techniques permitted us to identify a total of 26 major *N*-glycans expressed in the recombinant mouse EC-SOD produced in CHO cells. They comprise the most predominant structure, the disialylated complex core-fucosylated biantennary sugar chain, and 25 additional types of glycans, a high mannose sugar chain, and mono-, bi-, tri-, and tetra-antennary complex sugar chains exhibiting varying degrees of sialylation, which were all clearly shown to be present in the recombinant EC-SOD. Since EC-SOD has a single *N*-glycosylation site, the enzyme can be present in at least 26 kinds of glycoforms in its monomeric state. Each *N*-glycan identified in the recombinant mouse EC-SOD may have a distinct function as to the properties of EC-SOD, including enzyme activity, heparin binding, proteolytic stability, oligomeric structure formation and so on. This possibility awaits further evaluation in the future. We believe that the *N*-glycosylation profile of the recombinant mouse EC-SOD will be beneficial for elucidating the structure-function relationships of EC-SOD *N*-glycans.

Acknowledgements This work was supported in part by Grants-in-Aid for Scientific Research, No. 22590563 (to T.O.), and Scientific Research (A), No. 20249018, from the Ministry of Education, Culture, Sports, Science, and Technology of Japan; and Scientific Research Frontier Biomedical Science Underlying Organelle Network Biology, the Japan Society for the Promotion of Science (JSPS) Global COE (Center of Excellence) Program of Osaka University. We also thank Mr. Nicholas J. Halewood for editing this manuscript.

References

1. McCord, J.M., Fridovich, I.: Superoxide dismutase. An enzymic function for erythrocuprein (Hemocuprein). J Biol Chem **244**, 6049–6055 (1969)
2. Okado-Matsumoto, A., Fridovich, I.: Subcellular distribution of superoxide dismutases (SOD) in rat liver. J Biol Chem **276**, 38388–38393 (2001)
3. Chang, L.Y., Slot, J.W., Geuze, H.J., Crapo, J.D.: Molecular immunocytochemistry of the CuZn superoxide dismutase in rat hepatocyte. J Cell Biol **107**, 2169–2179 (1988)
4. Kawaguchi, T., Noji, S., Uda, T., Nakashima, Y., Takeyasu, A., Kawai, Y., Takagi, H., Tohyama, M., Taniguchi, N.: A monoclonal antibody against COOH-terminal peptide of human liver manganese superoxide dismutase. J Biol Chem **264**, 5762–5767 (1989)
5. Marklund, S.L.: Human copper-containing superoxide dismutase of high molecular weight. Proc Natl Acad Sci USA **79**, 7634–7638 (1982)
6. Peeker, R., Abramsson, L., Marklund, S.L.: Superoxide dismutase isoenzymes in human seminal plasma and spermatozoa. Mol Hum Reprod **3**, 1061–1066 (1997)
7. Marklund, S.L.: Product of extracellular-superoxide dismutase catalysis. FEBS Lett **184**, 237–239 (1985)
8. Karlsson, K., Lindahl, U., Marklund, S.L.: Binding of human extracellular superoxide dismutase C to sulphated glycosaminoglycans. Biochem J **256**, 29–33 (1988)
9. Marklund, S.L.: Extracellular superoxide dismutase in human tissues and human cell lines. J Clin Invest **74**, 1398–1403 (1984)
10. StrÖmqvist, M., Holgersson, J., Samuelsson, B.: Glycosylation of extracellular superoxide dismutase studied by high-performance liquid chromatography and mass spectrometry. J Chromatogr **548**, 293–301 (1991)
11. Angelove, M., Dolashka-Angelova, P., Ivanova, E., Serkedjieva, J., Slokoska, L., Pashova, S., Toshkova, R., Vassilev, S., Simeonov, I.: Hartmann, H-J., Stoeva, S., Weser, U., Voelter, W.: A novel glycosylated Cu/Zn-containing superoxide dismutase: production and potential therapeutic effect. Microbiology **147**, 1641–1650 (2001)
12. Dolashka-Angelova, P., Stevanovic, S., Dolashki, A., Angelova, M., Serkedjieva, J., Krumova, E., Pashova, S., Zacharieva, S., Voelter, W.: Structural and functional analysis of glycosylated Cu/Zn-superoxide disumutase from the fungal strain *Humicola lutea* 103. Biochem Biophys Res Commun **317**, 1006–1016 (2004)
13. Dolashka-Angelova, P., Moshtanska, V., Kujumdzieva, A., Atanasov, B., Petrova, V., Voelter, W., Van Beeumen, J.: Structure of glycosylated Cu/Zn-superoxide dismutase from *Kluyveromyces* yeast NBIMCC 1984. J Mol Struct **980**, 18–23 (2010)
14. Edlund, A., Edlund, T., Hjalmarsson, K., Marklund, S.L., SandstrÖm, J., StrÖmqvist, M., Tibell, L.: A non-glycosylated extracellular superoxide dismutase variant. Biochem J **288**, 451–456 (1992)
15. Mariño, K., Bones, J., Kattla, J.J., Rudd, P.M.: A systematic approach to protein glycosylation analysis: a path through the maze. Nat Chem Biol **6**, 713–723 (2010)
16. Varki, A.: Biological roles of oligosaccharides: all of the theories are correct. Glycobiology **3**, 97–130 (1993)
17. Dennis, J.W.: *N*-Acetylglucosaminyltransferase-V. In: Taniguchi, N., Honke, K., Fukuda, M. (eds.) Handbook of Glycosyltransferases and Related Genes, pp. 94–101. Springer, Tokyo (2002)
18. Nishimura, M., Ookawara, T., Eguchi, H., Fujiwara, N., Yoshihara, D., Yasuda, J., Mimura, O., Suzuki, K.: Inhibition of gene expression of heparin-binding epidermal growth factor-like growth factor by extracellular superoxide dismutase in rat aortic smooth muscle cells. Free Radic Res **40**, 589–595 (2006)
19. Laemmli, U.K.: Cleavage of structural proteins during the assembly of the head of bacteriophage T4. Nature **227**, 680–685 (1970)
20. Kondo, A., Suzuki, J., Kuraya, N., Hase, S., Kato, I., Ikenaka, T.: Improved method for fluorescence labeling of sugar chains with sialic acid residues. Agric Biol Chem **54**, 2169–2170 (1990)

21. Tokugawa, K., Oguri, S., Takeuchi, M.: Large scale preparation of PA-oligosaccharides from glycoproteins using an improved extraction method. Glycoconj J **13**, 53–56 (1996)
22. Fan, J.Q., Huynh, L.H., Lee, Y.C.: Purification of 2-aminopyridine derivatives of oligosaccharides and related compounds by cation-exchange chromatography. Anal Biochem **232**, 65–68 (1995)
23. Korekane, H., Shida, K., Murata, K., Ohue, M., Sasaki, Y., Imaoka, S., Miyamoto, Y.: Evaluation of laser microdissection as a tool in cancer glycomic studies. Biochem Biophys Res Commun **352**, 579–586 (2007)
24. Tomiya, N., Awaya, J., Kurono, M., Endo, S., Arata, Y., Takahasi, N.: Analyses of N-linked oligosaccharides using a two-dimensional mapping technique. Anal Biochem **171**, 73–90 (1988)
25. Makino, Y., Omichi, K., Hase, S.: Analysis of oligosaccharide structures from the reducing end terminal by combining partial acid hydrolysis and a two-dimensional sugar map. Anal Biochem **264**, 172–179 (1998)
26. Murakami, T., Natsuka, S., Nakakita, S., Hase, S.: Structure determination of a sulfated N-glycans, candidate for a precursor of the selectin ligand in bovine lung. Glycoconj J **24**, 195–206 (2007)
27. Misonou, Y., Shida, K., Korekane, H., Seki, Y., Noura, S., Ohue, M., Miyamoto, Y.: Comprehensive clinico-glycomic study of 16 colorectal cancer specimens: elucidation of aberrant glycosylation and its mechanistic causes in colorectal cancer cells. J Proteome Res **8**, 2990–3005 (2009)
28. Sali, A., Blundell, T.L.: Comparative protein modeling by satisfaction of spatial restraints. J Mol Biol **234**, 779–815 (1993)
29. Antonyuk, S.V., Strange, R.W., Marklund, S.L., Samar Hasnain, S.: The structure of human extracellular copper-zinc superoxide dismutase at 1.7Å resolution: Insights into heparin and collagen binding. J Mol Biol **388**, 310–326 (2009)
30. Consortium, T.U.: The universal protein resource (UniProt) in 2010. Nucleic Acid Res **38**, D142–148 (2010)
31. Folz, R.J., Guan, J., Seldin, M.F., Oury, T.D., Enghild, J.J., Crapo, J.D.: Mouse extracellular superoxide dismutase: primary structure, tissue-specific gene expression, chromosomal localization, and lung *in situ* hybridization. Am J Respir Cell Mol Biol **17**, 393–403 (1997)
32. Ookawara, T., Kizaki, T., Oh-ishi, S., Yamamoto, M., Matsubara, O., Ohno, H.: Purification and subunit structure of extracellular superoxide dismutase from mouse lung tissue. Arch Biochem Biophys **340**, 299–304 (1997)
33. Hemmerich, S., Leffler, H., Rosen, S.D.: Structure of the *O*-glycans in GlyCAM-1, an endothelial-derived ligand for L-selectin. J Biol Chem **270**, 12035–12047 (1995)
34. Taniguchi, N., Miyoshi, E., Gu, J., Honke, K., Matsumoto, A.: Decoding sugar chain functions by identifying target glycoproteins. Curr Opin Struct Biol **16**, 561–566 (2006)
35. Miyoshi, E., Taniguchi, N.: α6-Fucosyltransferase (FUT8). In: Taniguchi, N., Honke, K., Fukuda, M. (eds.) Handbook of Glycosyltransferases and Related Genes, pp. 259–263. Springer, Tokyo (2002)
36. Minowa, M.T., Oguri, S., Yoshida, A., Takeuchi, M.: N-Acetylglucosaminyltransferase-IV. In: Taniguchi, N., Honke, K., Fukuda, M. (eds.) Handbook of Glycosyltransferases and Related Genes, pp. 87–93. Springer, Tokyo (2002)
37. Ihara, S., Miyoshi, E., Nakahara, S., Sakiyama, H., Ihara, H., Akinaga, A., Honke, K., Dickson, R.B., Lin, C.Y., Taniguchi, N.: Addition of β1-6 GlcNAc branching to the oligosaccharide attached to Asn 772 in the serine protease domain of matriptase plays a pivotal role in its stability and resistance against trypsin. Glycobiology **14**, 139–146 (2003)
38. Hjalmarsson, K., Marklund, S.L., Engström, A., Edlund, T.: Isolation and sequence of complementary DNA encoding human extracellular superoxide dismutase. Proc Natl Acad Sci USA **84**, 6340–6344 (1987)
39. Due, A.V., Petersen, S.V., Valnickova, Z., Østergaard, L., Oury, T. D., Crapo, J.D., Enghild, J.J.: Extracellular superoxide dismutase exists as an octamer. FEBS Lett **580**, 1485–1489 (2006)
40. Kinnula, V.L., Crapo, J.D.: Superoxide dismutases in the lung and human lung diseases. Am J Respir Crit Care Med **167**, 1600–1619 (2003)
41. Oury, T.D., Day, B.J., Crapo, J.D.: Extracellular superoxide dismutase in vessels and airways of humans and baboons. Free Radic Biol Med **20**, 957–965 (1996)
42. Ookawara, T., Imazeki, N., Matsubara, O., Kizaki, T., Oh-ishi, S., Nakano, C., Sato, Y., Ohno, H.: Tissue distribution of immunoreactive mouse extracellular superoxide dismutase. Am J Physiol **275**, C840–C847 (1998)
43. Carlsson, L.M., Jonsson, J., Edlund, T., Marklund, S.L.: Mice lacking extracellular superoxide dismutase are more sensitive to hyperoxia. Proc Natl Acad Sci USA **92**, 6264–6268 (1995)
44. Jung, O., Marklund, S.L., Geiger, H., Pedrazzini, T., Busse, R., Brandes, R.P.: Extracellular superoxide dismutase is a major determinant of nitric oxide bioavailability: In vivo and ex vivo evidence from ecSOD-deficient mice. Circ Res **93**, 622–629 (2003)
45. Chu, Y., Alwahdani, A., Iida, S., Lund, D.D., Faraci, F.M., Heistad, D.D.: Vascular effects of the human extracellular superoxide dismutase R213G variant. Circulation **112**, 1047–1053 (2005)
46. Yao, H., Arunachalam, G., Hwang, J.-W., Chung, S., Sundar, I.K., Kinnula, V.L., Crapo, J.D., Rahman, I.: Extracellular superoxide dismutase protects against pulmonary emphysema by attenuating oxidative fragmentation of ECM. Proc Natl Acad Sci USA **107**, 15571–15576 (2010)
47. Wang, X., Inoue, S., Gu, J., Miyoshi, E., Noda, K., Li, W., Mizuno-Horikawa, Y., Nakano, M., Asahi, M., Takahashi, M., Uozumi, N., Ihara, S., Lee, S.H., Ikeda, Y., Yamaguchi, Y., Aze, Y., Tomiyama, Y., Fujii, J., Suzuki, K., Kondo, A., Shapiro, S.D., Lopez-Otin, C., Kuwaki, T., Okabe, M., Honke, K., Taniguchi, N.: Dysregulation of TGF-β1 receptor activation leads to abnormal lung development and emphysema-like phenotype in core fucose-deficient mice. Proc Natl Acad Sci USA **102**, 15791–15796 (2005)